IEEE Access
Multidisciplinary | Rapid Review | Open Access Journal

Received May 7, 2021, accepted May 14, 2021, date of publication May 17, 2021, date of current version June 1, 2021.

Digital Object Identifier 10.1109/ACCESS.2021.3081435

Characterization Method of Surface Crack Based on Laser Thermography

JIAQI LIU[1], ZHIJIE ZHANG[1], (Member, IEEE), ZHENYU LIN[1], HAOZE CHEN[1], AND WULIANG YIN[1,2], (Senior Member, IEEE)

[1]School of Instrument and Electronics, North University of China, Taiyuan 030051, China
[2]School of Electrical and Electronic Engineering, University of Manchester, Manchester M13 9PL, U.K.

Corresponding author: Zhijie Zhang (zhangzhijie@nuc.edu.cn)

This work was supported by the Fund for Shanxi 1331 Project Key Subject Construction of China.

ABSTRACT The characterization of micro cracks on metal surface plays an important role in the process of manufacturing and using, which has attracted a lot of attention. This is mainly due to the fact that the size of defects is smaller and the depth of defects is difficult to predict compared with metal materials with larger plane, which is still challenging. In order to solve this problem, this paper proposes a characterization method of surface defects based on reflective laser thermography, and designs a laser heating nondestructive testing system based on reflection. The system includes a semiconductor laser to heat the surface of metal cracks, and an infrared imager to record changes in the temperature field of the metal surface. In the process of data analysis, an Otsu adaptive threshold segmentation method is selected to quantify the defect size, which can control the quantification accuracy of defect size within 25%. A derivative analysis method is proposed to quantify the depth of defects, which can control the depth quantification accuracy of tiny defects within 7%.

INDEX TERMS Characterization, micro cracks, laser thermography, nondestructive testing.

I. INTRODUCTION

The blades of heavy-duty gas turbines, aero engines, etc. can work under high temperature, high pressure, and high speed environments [1], [2]. But in this extreme case, the performance and wear of the blades will accelerate degradation and lead to defects, resulting in major failures and economic losses. Among these major failures, blade fracture occupies a considerable part of the cause, and blade fracture is mainly caused by surface cracks. In order to ensure the reliability of the blade, it is particularly important to regularly detect and quantify the defects on the blade surface [3]. Due to efficiency issues and time cost issues, it has become more and more necessary to propose an effective and fast method.

In recent years, Non-destructive testing (NDT) techniques have been widely used to detect surface defects and have achieved good results [4]. NDT is a technology that detects the object under test without affecting its performance [5]. It has the advantages of non-destructive, comprehensive, and full-process. In order to use NDT technology for surface defect detection, a variety of excitation methods have been proposed to detect surface defects, such as eddy current testing [6], [7], ultrasonic testing [8], radiographic testing (RT) [9], infrared thermography testing etc [10], and active infrared thermography detection technology [11] has been widely used in the field of surface defect detection due to its non-contact, fast detection speed, high sensitivity, and real-time detection.

Active infrared thermography technology is a fast, non-contact detection method. The method can be divided into halogen lamp excitation [12], eddy current excitation [13], laser excitation [14], ultrasonic excitation [15], microwave excitation [16], resistive heating and mechanical vibrations excitation according to different heating excitation. And this method can be divided into reflection type and transmission type due to the different placement of the infrared imager. Liu Zewei and others proposed an eddy current pulse thermography system based on L-shaped electromagnetic induction thermography, which is used to inspect metal materials with irregular geometrical cracks, But this excitation method is only suitable for conductive materials [17]. Moskovchenko *et al.* used pulsed laser thermography to detect translucent composite materials, discussed the feasibility of laser detection of translucent composite materials,

The associate editor coordinating the review of this manuscript and approving it for publication was Laurence T. Yang.

and used neural networks to evaluate the depth of defects of the tested materials, the paper did not characterize the size of the defect [18]. C. Cavallone *et al.* used ultrasonic-induced infrared thermography detection technology to determine the length of surface cracks and inspected the material to verify its effectiveness. However, the directivity of this excitation method is poor, and it is not obvious to detect smaller defects [19]. Wang Zijun *et al.* compared eddy current pulse thermography technology and long pulse thermography technology, and the results showed that long pulse thermography technology has better advantages in detecting low thermal conductivity materials [20]. Sannikov *et al.* used resistance heating to detect defects in steel bars, but did not characterize the size of the defects [21]. Liu bin *et al.* used vibration heating to detect defects in composite materials. This method is likely to damage the sample when detecting deeper defects [22]. In the field of 3D characterization, SS Pawar *et al.* used a 3D normalization approach to 3D characterization of defects in composite materials, but this method only characterizes the shape of the defect, and does not quantify the shape, size, and depth of the defect [23]. During this period, many researchers used deep learning method in the field of defect detection. Cha YoungJin *et al.* used deep learning methods to detect defects in concrete and studied the existence of defects [24]. In order to detect multiple types of defects simultaneously, cha youngjin *et al.* proposed a faster Region-based Convolutional Neural Network (Faster R-CNN)-based structural visual inspection method. This method only classifies different types of defects [24]. Rahmat Ali *et al.* used a combination of thermal imaging cameras and deep learning to detect damage to steel structures. This method has limitations in detecting small defects in steel structures [25]. GH Beckman *et al.* used a depth camera to quantify the volume of the defect shed on the concrete surface. When a tiny defect exists, the depth camera cannot collect the details of the tiny defect, so the method in this article has limitations in the characterization of the tiny defect [26]. It can be seen from the above research that active infrared thermography technology has made considerable progress. However, in the traditional thermal excitation method, the limitations of the tested material, poor intuition, and high energy consumption have affected the development of non-destructive testing. In the research field of deep learning, scholars have classified and predicted the existence of defects, the types of defects, and the depth of defects. In the field of infrared image processing. Wang Fei *et al.* proposed an image separation technology based on wavelet transform to detect the degumming defects of the engine and calculate the size of the defects [27]. Wen ChingMei *et al.* proposed a thermal image data analysis method, which uses principal component analysis to reduce the dimensionality of the collected thermal images and extract defects [28]. So far, there is still a lack of a method to quantitatively characterize the shape, size, and depth of metal defects. In this paper, a reflection-based laser thermography system is built and a reflection-based laser thermography method is used to perform quantitative characterization of micro cracks on metal surfaces to evaluate surface micro cracks. In this system, the laser is used to heat the vicinity of the defect, and the infrared thermal imager is used to collect the surface temperature field of the material.

In this work, the second part analyzes the thermal diffusion principle of temperature. In the third section, experiments were carried out with structural steel as the test piece, and analyzes the data collected by the system. The fourth section introduces the conclusion of this article.

II. THEORETICAL FUNDAMENTALS

We need to assume that the test piece is a semi-infinite object. During the laser heating process, the light energy of the laser is irradiated on the test piece, and the light energy of the laser will be divided into three parts [29]:

$$E + R + T = 1 \tag{1}$$

where, E is the ratio of the energy absorbed by the material in the laser irradiation process to the laser light energy, R is the ratio of the reflected energy to the laser light energy in the laser irradiation process, T is the ratio of transmitted energy to laser light energy during laser irradiation. When the wavelength of the laser is constant, the reflectivity and emissivity of the material are constant. When the material is opaque, the transmittance is 0.

This article uses reflective laser thermography technology to detect defects on the material surface. The laser point heat source is used as the light source. In the process of laser working, the distribution of laser energy obeys Gaussian distribution [30]:

$$I_0 = \frac{P}{\pi \times r^2} \exp\left(\frac{x^2 + y^2}{-r^2}\right) \tag{2}$$

where, P is the output power of the laser. r is the laser spot radius. I_0 is the laser intensity, x and y are the coordinates of other points when the laser heating point is the origin of the coordinates.

During the laser heating process, the specimen receives the radiant energy, and the heating function of the laser heat source is:

$$Q(x, y, z, t) = EI_0\mu \exp(-\mu z) \tag{3}$$

where, μ is the linear absorption coefficient of the material to the laser:

$$\mu = 4\pi\kappa/\lambda_0 \tag{4}$$

where, λ_0 is the wavelength of the laser, κ is the extinction coefficient.

When the laser heats the material, the heat will diffuse from the heating point in different directions, and flow from the higher temperature area to the lower temperature area, and finally the temperature field will reach thermal equilibrium. When the heat source of laser heating is $Q(x, y, z, t)$, The

heat transfer equation in the 3D Cartesian coordinate system is [31]:

$$\rho C_p \frac{\partial T}{\partial t} - \alpha_x \frac{\partial^2 T}{\partial x^2} + \alpha_y \frac{\partial^2 T}{\partial y^2} + \alpha_z \frac{\partial^2 T}{\partial z^2} = Q(x, y, z, t) \quad (5)$$

where, ρ is the density, C_p is Specific heat capacity, α_x, α_y, α_z are the thermal diffusivity of the material in different directions. When the material is the same and there are no defects:

$$\alpha_x = \alpha_y = \alpha_z = \frac{\lambda}{\rho C_p} \quad (6)$$

where, λ is Thermal conductivity.

When the material is heated by laser, the temperature inside the material is

$$T(x, y, z, t) = \frac{Q(x, y, z, t)}{4\pi\lambda t} \exp\left(\frac{\left(x^2 + y^2 + z^2\right)}{4\alpha t}\right) + C_0 \quad (7)$$

where, C_0 is a constant coefficient and related to the ambient temperature. It can be seen from Equation 7 that the thermal diffusion change of the material is related to the thermal diffusivity and thermal conductivity. When a defect exists, the thermal conductivity and thermal diffusivity of the defect will change. At the same time, the inner wall of the defect will increase the reflection of the laser, so the surface temperature of the material defect will be different.

This paper collects the temperature field distribution on the heating side surface of the material, and the heat will diffuse along the surroundings. When there are no cracks on the tested surface of the material, the density, specific heat capacity, and thermal conductivity of the material will not change, the thermal diffusivity of the tested piece is the same, and the temperature field of the material surface changes regularly. When cracks appear on the material surface, various parameters of the material at the defect will be affected, and the temperature field of the material surface will change. At this time, the three-dimensional characterization of the material defect can be obtained by analyzing the temperature field of the material surface.

III. TEST SYSTEM AND METHOD

The infrared thermography system built in this article is shown in Fig.1. The system includes a computer, an infrared thermal imager, a semiconductor laser, a Fourier lens, and a signal generator. The infrared thermal imager adopts the fast m200 imager of Canada TELOPS company. The laser chooses the RFL-A1000D laser of Wuhan Ruike, and the laser can output laser with a power range of 0 to 550w. Fourier lens is used to adjust the laser spot radius. The signal generator is used to control the output time of the laser. The computer is used to process the images collected by the infrared camera.

In this study, structural steel was selected as the tested material, and the size of the material was $290\times200\times2.6\,\text{mm}^3$, the characteristics of the tested material are shown in Fig.2.

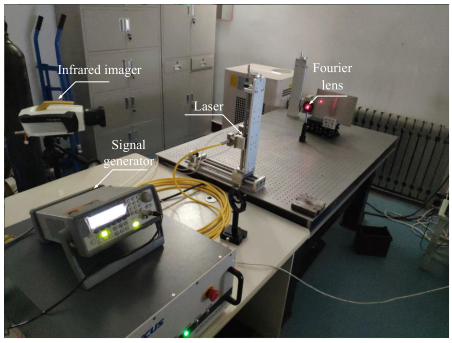

FIGURE 1. Infrared thermography system.

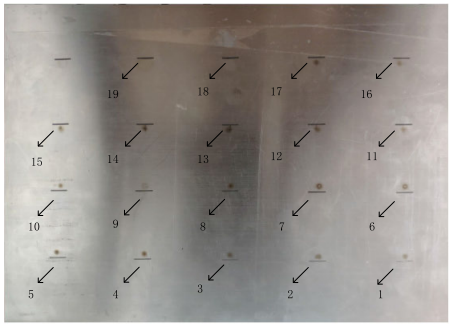

FIGURE 2. Structural steel.

There were 19 defects on the surface of the material, the surface size of the defects was $0.5\times10\,\text{mm}^2$, and the defect depth increased. The depth of the first defect was 0.13 mm. With the increase of the serial number, the defect depth increased at intervals of 0.13 mm. In the nineteenth defect, the defect depth was 2.47 mm.

First, the test system needs to be adjusted. We need to move the optical lens and adjust the laser spot radius to 1.5mm; then we need to adjust the laser power to 50W, and then we set the output signal of the signal generator to make the laser output time of the laser 1s. Then we placed the thermal imaging camera on the side of the laser, and placed the thermal imaging camera at a distance of 1.36m from the measured object. Finally we turn on the laser to heat the surface of the material. During the heating process, an infrared thermal imager is used to record the changes in the temperature field on the surface of the material.

First of all, it is necessary to determine whether the crack exists and the size of the cracks.

The data collected by the infrared thermal imager is a 3D image matrix, which is composed of n $M * N$ 2D matrices:

$$\boldsymbol{A}_P = \begin{bmatrix} a_{11} & \cdots & a_{1N} \\ \vdots & \ddots & \vdots \\ a_{M1} & \cdots & a_{MN} \end{bmatrix}, \quad P = 1, 2, \ldots, n \quad (8)$$

Among the n 2D matrices, due to the different heating time, there is a difference that the contrast of the defect is not obvious. In order to make the contrast of the defect more obvious, we choose the two-dimensional matrix image with the highest heating temperature as the experimental matrix. The experimental image is shown in Figure 3.

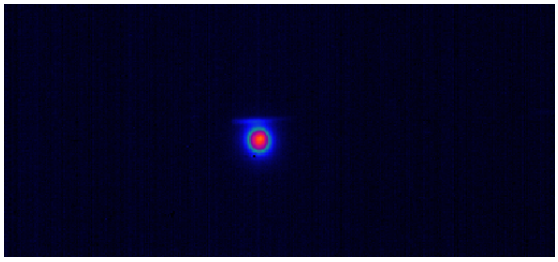

FIGURE 3. Experimental image.

It can be seen from Fig. 3 that when the crack does not exist, the temperature field change will decrease uniformly, and when there is a crack above the laser heating point, the temperature of the defect will increase significantly, so the defect can be located.

When the defect exists, the size and depth of the defect becomes a more difficult problem. First, we need to move the laser heating point to 15 pixels below the middle of the defect, and then we traverse and heat 19 defects. Each movement requires 0.5s, and the temperature field data of each defect needs to be collected for 2s. In the entire data collection process, a total of 47.5s is required. During the traversal process, we collect the temperature field data of each defect

In the heat dissipation process, the area without defects is uniformly dissipated, and the heat dissipation rate of the defects is slow, so the infrared image during the heat dissipation process is used as the measured image to quantify the defect size.

During heat dissipation, the infrared images corresponding to defects of different depths are shown in Fig. 4.

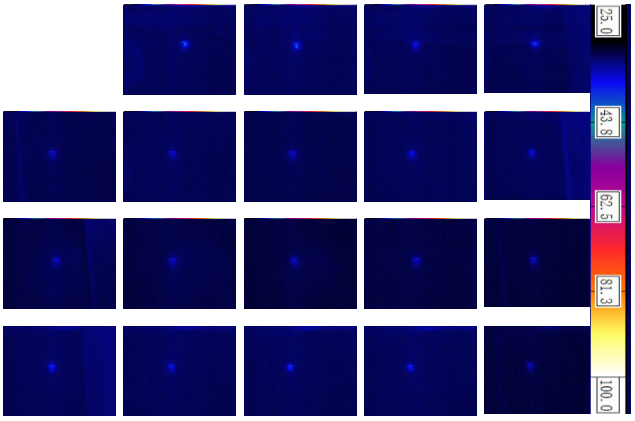

FIGURE 4. Infrared images corresponding to defects of different depths.

When the defect depth is 0.13mm, the 3D representation of the infrared image is shown in Figure 5.

It can be seen from Fig. 5 that the heat at the laser source has been evenly dissipated, and the heat diffusion rate at the crack will be relatively slow. At the same time, the probability of pixel values being divided into two categories is p_1 and p_2. In order to extract the defect area in the infrared image, it is necessary to select a threshold to perform threshold segmentation on the infrared image. In traditional binarization segmentation algorithms, a fixed value is usually selected

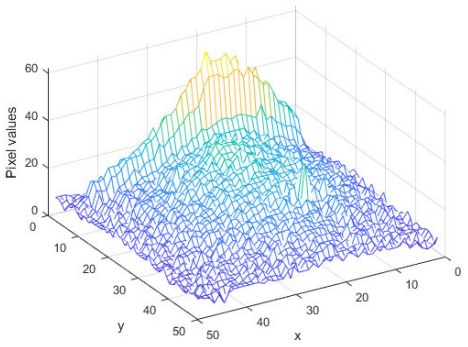

FIGURE 5. The 3D representation of the temperature field when the crack depth is 0.13mm.

as the segmentation threshold. However, these methods have limitations. When the gray levels of the divided regions in the image are different, the divided regions in the image will be filtered out. At this point, we need to use a method to calculate the threshold in the image in real time, and use the threshold to segment the image. Otsu algorithm is an adaptive threshold segmentation method. First, calculate the segmentation threshold of the image according to the different characteristics of the infrared image, and then perform the optimal segmentation of the image, and the defects in the image will be completely extracted.

Therefore, this article first chooses the Otsu algorithm to segment the measured image. Otsu algorithm is called the maximum between-class variance method. This method assumes that there is a threshold in the image that can divide all pixels into two categories. Then the pixel mean values of these two types of pixels are m_1 and m_2, and the global mean value of the image is mG. So:

$$p_1^* m_1 + p_2^* m_2 = mG \tag{9}$$

$$p_1 + p_2 = 1 \tag{10}$$

The between-class variance is:

$$\sigma^2 = p_1(m_1 - mG)^2 + p_2(m_2 - mG)^2 \tag{11}$$

Substitute formula 1 into formula 3:
Among them:

$$p_1 = \sum_{i=0}^{k} p_i \tag{12}$$

$$m_1 = 1/p1 * \sum_{i=0}^{k} ip_i \tag{13}$$

$$m_2 = 1/p_2 * \sum_{i=k+1}^{L-1} ip_i \tag{14}$$

The gray value k that maximizes the variance in formula 14 is the threshold.

The image after threshold segmentation is shown in Fig. 6.

It can be seen from Fig. 6 that the contour of the defect and the contour of the laser heating point have been clearly characterized. Then filter out the influence of the laser heating

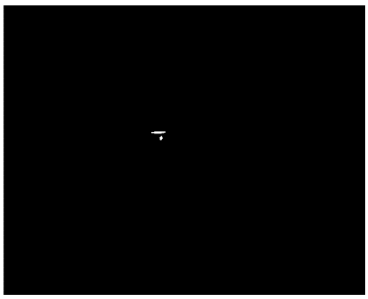

FIGURE 6. Image after threshold segmentation.

point, and filter out the area with a smaller contour area. The processed image is shown in Fig. 7.

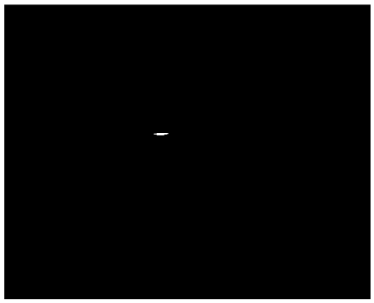

FIGURE 7. Processed image.

Next, it is necessary to characterize the defect shape. The bwboundaries function in Matlab is used to extract the shape of the crack. The function uses 8 fields to extract the contour of the defect, and then uses the smallest bounding rectangle to distinguish the contour. The processed image is shown in Fig. 8.

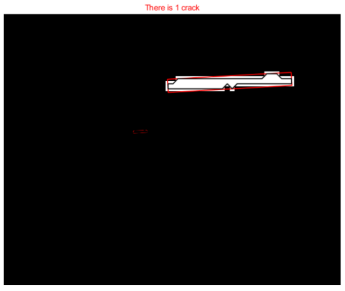

FIGURE 8. Image after contour representation.

Then characterize the size of the crack profile. The size of each pixel under the object distance needs to be calculated. When the object distance is 1.35m, the set spatial resolution is 640*512, and the size of the resulting object is 16cm*12.8cm. It can be seen that at this object distance, the size of a single pixel is 0.25mm*0.25mm.

Then the number of pixels in the connected domain is calculated. The number of pixels is determined by observing the 2*2 area. When there are 0 pixels with a value of 0 around the area, the area of this point is 0. When there is 1 pixel with zero value around the area, the area is 0.25. When there are 2 adjacent zero-value pixels around the area, the area is 0.5. When there are 2 diagonal zero-value pixels around the area, the area is 0.75. When there are 3 zero-value pixels around the area, the area is 0.8775. When there are 4 pixels with zero value around the area, the area is 1. This method is used to determine the number of pixels in the connected domain to determine the size of the surface cracks. The number of pixels contained in defects at different depths are shown in Fig. 9.

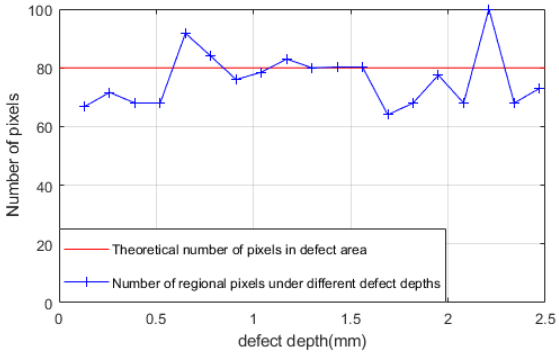

FIGURE 9. The number of pixels contained in defects at different depths.

It can be seen from Fig. 9 that as the depth of the defect increases, the number of pixels in the defect is basically maintained at about 80, and does not change drastically as the depth of the defect increases. The method in this paper can control the quantization error of micro-cracks within 25%, and the method can also characterize the shape of the cracks.

After the size of the defect is characterized, classifying the depth of the defect becomes a problem that must be solved.

Theoretical analysis shows that when there is a defect on the surface of the material, the inner wall of the defect will increase the temperature of the defect due to the reflection of the laser, and the temperature change trend at the edge of the defect will also become steep. Therefore, this paper chooses the method of derivative analysis to classify the defect depth of the material. The schematic diagram of this method is shown in Fig.10.

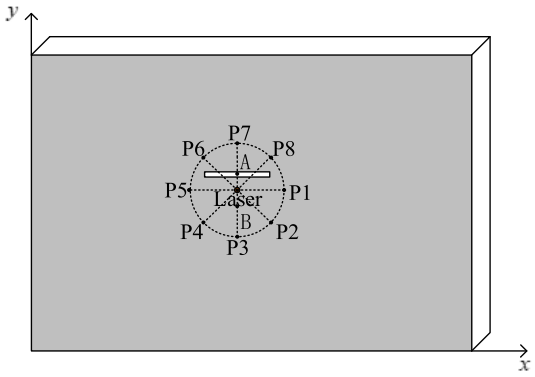

FIGURE 10. The schematic diagram of this method.

This method collects temperature curves for p1-p5, p2-p6, p3-p7, p4-p8 line segments at a certain heating time, and then performs derivative transformation on the temperature curves of these line segments:

$$D_{l-n} = diff\ (G_{l-n}) \tag{15}$$

where, G_{l-n} is the gray value data from the laser to Pn, D_{l-n} is the gray value data of G_{l-n} after the derivative, Then the difference analysis of the two line segments on the same line after the derivative is carried out, and the maximum value of the difference in the line segment is extracted. Finally, the maximum value is used to quantify the defect depth:

$$D_n = \max\left(|D_{l-n+4} - D_{l-n}|\right) \tag{16}$$

where, D_n is the maximum difference of derivative.

When the heating time is 1 s, the temperature field data on the eight line segments shown in the figure above are collected.

When the crack depth is 0.13mm, the gray value change curves of four line segments are shown in Fig. 11.

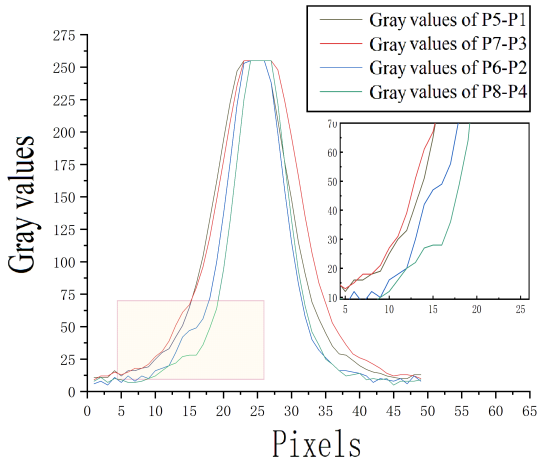

FIGURE 11. Gray value change curves of four line segments.

It can be seen from Fig.11 that when there is no crack, G_{5-1} becomes a steady upward trend. When a crack exists, the temperature change at the crack becomes a convex state. In order to extract the temperature change at the crack, the derivative of the temperature change curve of the line segment is performed, as shown in Fig.12.

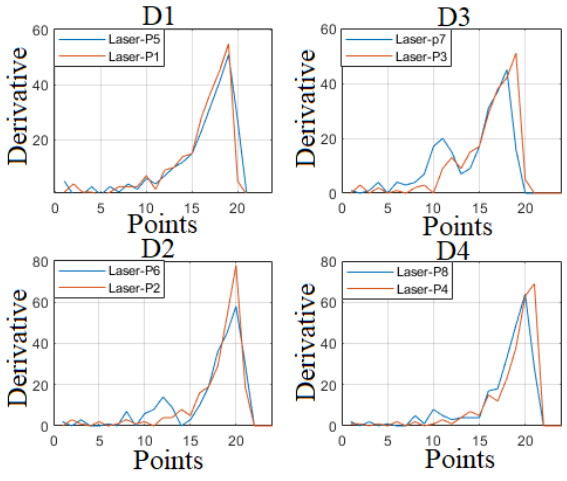

FIGURE 12. The derivative of the temperature change curve of the line segment.

It can be seen from Fig.12 that when there is no crack, the temperature change trend on both sides of the laser heating point is roughly the same. When a crack exists, the derivative on both sides of the laser heating point will be different.

The defect is located at the pixel points 10-15, and the derivative of the two line segments on both sides of the laser heating point is made difference. Therefore, the maximum value of the difference between the pixel points 10-15 is extracted. The maximum value of the difference under different defect depths is shown in Fig. 13.

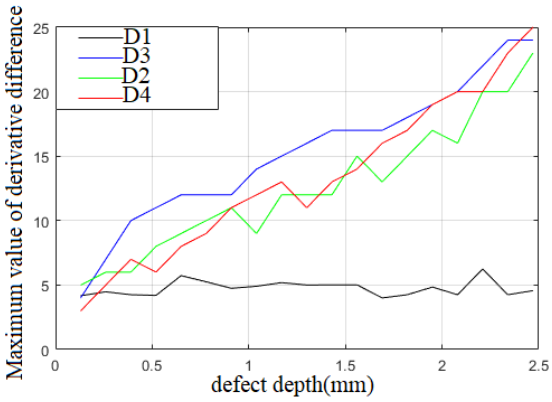

FIGURE 13. Maximum value of the difference under different defect depths.

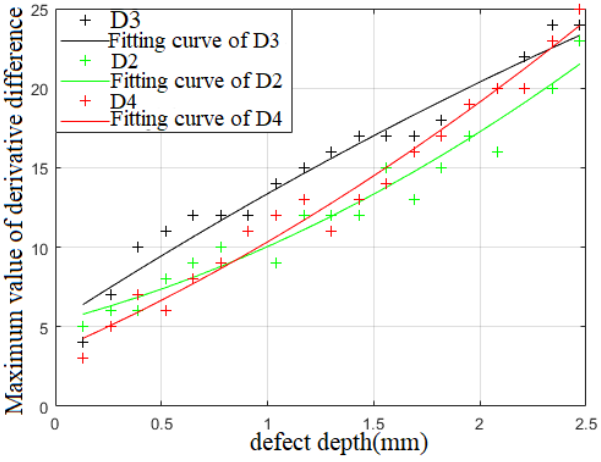

FIGURE 14. Fitted curves.

TABLE 1. The various index parameters of the fitted curve.

Fitted curve	RMSE	R-square	Detection accuracy error(%)
$D2$=1.247*x^2+3.477*x+5.318	1.1594	0.9535	6.29%
$D3$=-0.5321*x^{2}8.617*x+5.283	1.1431	0.9601	6.29%
$D4$=-0.9727*x^2+5.879*x+3.484	1.0335	0.9756	5.68%

It can be seen from Fig. 13 that when the heating time is 1s, with the increasing defect depth, the D_1 basically remains stable and does not show a trend of regular changes, D_2, D_3 and D_4 will increase with the continuous improvement of defect depth. Next, quadratic function is used to fit the

extreme value of the derivative difference and the depth of the defect. The fitted curves are shown in Fig. 14.

The various index parameters of the fitted curves are shown in Table 1.

It can be seen from Table 1 that different fitting curves can control the detection accuracy of defect depth within 7%.

IV. CONCLUSION

Aiming at the characterization of small defects on metal surfaces, a reflective laser thermography system was constructed. Through the analysis of the temperature field changes on the surface of the defect, the defect can be characterized. In order to detect the surface area of the defect, the image in the cooling process is selected as the measured image, and an Otsu adaptive threshold segmentation method is used to process the measured image and extract the surface area of the defect. The results show that the defect size detection accuracy of this method at different defect depths can be controlled within 25%. Aiming at the depth detection of surface defects, a derivative analysis method is proposed, which analyzes the derivative of the temperature field on the surface of the defect, and records the maximum value of the derivative difference. The data shows that the maximum value of the derivative difference increases with the continuous increase of the defect depth. Finally, the second order function is used to fit the maximum value of defect depth and derivative difference. The results show that the precision of depth detection can be controlled within 7 % by this method.

REFERENCES

[1] Z. Tong, S. Xie, H. Liu, W. Zhang, C. Pei, Y. Li, Z. Chen, T. Uchimoto, and T. Takagi, "An efficient electromagnetic and thermal modelling of eddy current pulsed thermography for quantitative evaluation of blade fatigue cracks in heavy-duty gas turbines," *Mech. Syst. Signal Process.*, vol. 142, Aug. 2020, Art. no. 106781.

[2] B. Zhou, F. Yu, Y. Luo, and H. Li, "Detecting defects in the main spar of a wind turbine blade," *J. Renew. Sustain. Energy*, vol. 12, no. 5, Sep. 2020, Art. no. 053304.

[3] Y. Du, S. Zhou, X. Jing, Y. Peng, H. Wu, and N. Kwok, "Damage detection techniques for wind turbine blades: A review," *Mech. Syst. Signal Process.*, vol. 141, Jul. 2020, Art. no. 106445.

[4] V. P. Vavilov and D. D. Burleigh, "Review of pulsed thermal NDT: Physical principles, theory and data processing," *NDT & E Int.*, vol. 73, pp. 28–52, Jul. 2015.

[5] Y.-K. Zhu, G.-Y. Tian, R.-S. Lu, and H. Zhang, "A review of optical NDT technologies," *Sensors*, vol. 11, no. 8, pp. 7773–7798, Aug. 2011.

[6] F. Yuan, Y. Yu, B. Liu, and G. Tian, "Investigation on velocity effect in pulsed eddy current technique for detection cracks in ferromagnetic material," *IEEE Trans. Magn.*, vol. 56, no. 9, pp. 1–8, Sep. 2020.

[7] C. Xu, W. Zhang, C. Wu, J. Xie, X. Yin, and G. Chen, "An improved method of eddy current pulsed thermography to detect subsurface defects in glass fiber reinforced polymer composites," *Compos. Struct.*, vol. 242, Jun. 2020, Art. no. 112145.

[8] F. Honarvar and A. Varvani-Farahani, "A review of ultrasonic testing applications in additive manufacturing: Defect evaluation, material characterization, and process control," *Ultrasonics*, vol. 108, Dec. 2020, Art. no. 106227.

[9] L. Morgan, "Testing defects in automated ultrasonic testing and radiographic testing," *Insight, Non-Destructive Test. Condition Monitor.*, vol. 60, no. 11, pp. 606–612, Nov. 2018.

[10] V. Kher and R. Mulaveesala, "Probability of defect detection in pulse compression favourable thermal excitation schemes for infra-red non-destructive testing," *Electron. Lett.*, vol. 56, no. 19, pp. 998–1000, Sep. 2020.

[11] S. Doshvarpassand, C. Wu, and X. Wang, "An overview of corrosion defect characterization using active infrared thermography," *Infr. Phys. Technol.*, vol. 96, pp. 366–389, Jan. 2019.

[12] Y. Xu, S. Hwang, Q. Wang, D. Kim, C. Luo, J. Yang, and H. Sohn, "Laser active thermography for debonding detection in FRP retrofitted concrete structures," *NDT & E Int.*, vol. 114, Sep. 2020, Art. no. 102285.

[13] F. Liu, J. Zhu, G. Y. Tian, C. Ulianov, and Z. Wang, "Investigations for inclination angle characterization of angular defects using eddy current pulsed thermography," *Infr. Phys. Technol.*, vol. 100, pp. 73–81, Aug. 2019.

[14] G. Inglese, R. Olmi, and A. Scalbi, "Characterization of a vertical crack using laser spot thermography," *Inverse Problems Sci. Eng.*, vol. 28, no. 8, pp. 1191–1208, Aug. 2020.

[15] V. P. Vavilov, A. A. Karabutov, A. O. Chulkov, D. A. Derusova, A. I. Moskovchenko, E. B. Cherepetskaya, and E. A. Mironova, "Comparative study of active infrared thermography, ultrasonic laser vibrometry and laser ultrasonics in application to the inspection of graphite/epoxy composite parts," *Quant. Infr. Thermogr. J.*, vol. 17, no. 4, pp. 235–248, Oct. 2020.

[16] A. Foudazi, A. Mirala, M. T. Ghasr, and K. M. Donnell, "Active microwave thermography for nondestructive evaluation of surface cracks in metal structures," *IEEE Trans. Instrum. Meas.*, vol. 68, no. 2, pp. 576–585, Feb. 2019.

[17] Z. Liu, B. Gao, and G. Y. Tian, "Natural crack diagnosis system based on novel L-shaped electromagnetic sensing thermography," *IEEE Trans. Ind. Electron.*, vol. 67, no. 11, pp. 9703–9714, Nov. 2020.

[18] A. I. Moskovchenko, V. P. Vavilov, R. Bernegger, C. Maierhofer, and A. O. Chulkov, "Detecting delaminations in semitransparent glass fiber composite by using pulsed infrared thermography," *J. Nondestruct. Eval.*, vol. 39, no. 3, pp. 1–10, Sep. 2020.

[19] C. Cavallone, M. Colom, A. Mendioroz, A. Salazar, D. Palumbo, and U. Galietti, "Sizing the length of surface breaking cracks using vibrothermography," *NDT & E Int.*, vol. 112, Jun. 2020, Art. no. 102250.

[20] Z. Wang, J. Zhu, G. Tian, and F. Ciampa, "Comparative analysis of eddy current pulsed thermography and long pulse thermography for damage detection in metals and composites," *NDT & E Int.*, vol. 107, Oct. 2019, Art. no. 102155.

[21] D. Sannikov, A. Kolevatov, V. Vavilov, and M. Kuimova, "Evaluating the quality of reinforced concrete electric railway poles by thermal nondestructive testing," *Appl. Sci.*, vol. 8, no. 2, p. 222, Feb. 2018.

[22] B. Liu, H. Zhang, H. Fernandes, and X. Maldague, "Experimental evaluation of pulsed thermography, lock-in thermography and vibrothermography on foreign object defect (FOD) in CFRP," *Sensors*, vol. 16, no. 5, p. 743, May 2016.

[23] S. S. Pawar and V. P. Vavilov, "Applying the heat conduction-based 3D normalization and thermal tomography to pulsed infrared thermography for defect characterization in composite materials," *Int. J. Heat Mass Transf.*, vol. 94, pp. 56–65, Mar. 2016.

[24] Y.-J. Cha, W. Choi, and O. Büyüköztürk, "Deep learning-based crack damage detection using convolutional neural networks," *Comput.-Aided Civil Infrastruct. Eng.*, vol. 32, no. 5, pp. 361–378, May 2017.

[25] R. Ali and Y.-J. Cha, "Subsurface damage detection of a steel bridge using deep learning and uncooled micro-bolometer," *Construct. Building Mater.*, vol. 226, pp. 376–387, Nov. 2019.

[26] G. H. Beckman, D. Polyzois, and Y.-J. Cha, "Deep learning-based automatic volumetric damage quantification using depth camera," *Autom. Construct.*, vol. 99, pp. 114–124, Mar. 2019.

[27] F. Wang, J. Liu, B. Dong, J. Gong, W. Peng, Y. Wang, M. Chen, and G. Liu, "Blind image separation for the debonding defects recognition of the solid propellant rocket motor cladding layer using pulse thermography," *Measurement*, vol. 174, Apr. 2021, Art. no. 108997.

[28] C.-M. Wen, S. Sfarra, G. Gargiulo, and Y. Yao, "Thermographic data analysis for defect detection by imposing spatial connectivity and sparsity constraints in principal component thermography," *IEEE Trans. Ind. Informat.*, vol. 17, no. 6, pp. 3901–3909, Jun. 2021.

[29] J. Meseguer, I. Pérez-Grande, and A. Sanz-Andrés, *Thermal Radiation Heat Transfer: Spacecraft Thermal Control*. 2012, pp. 73–86.

[30] P. Yu and Y. Zeng, "Characterization of laser-induced local heating in a substrate," *Int. J. Heat Mass Transf.*, vol. 106, pp. 989–996, Mar. 2017.

[31] N. Puthiyaveettil, K. R. Thomas, S. Unnikrishnakurup, P. Myrach, M. Ziegler, and K. Balasubramaniam, "Laser line scanning thermography for surface breaking crack detection: Modeling and experimental study," *Infr. Phys. Technol.*, vol. 104, Jan. 2020, Art. no. 103141.

JIAQI LIU was born in Shuozhou, Shanxi, China, in 1997. He received the bachelor's degree in measuring techniques and instruments from the North University of China. He is currently pursuing the master's degree in instrumentation engineering with North China University. Since 2018, he has been engaged in the research of image processing and signal processing.

ZHIJIE ZHANG (Member, IEEE) was born in Taiyuan, Shanxi, China, in 1965. He received the bachelor's degree in automation instrumentation from Tianjin University, the master's degree in testing technology from the Taiyuan Mechanical Institute (currently the North University of China), in 1989, and the Ph.D. degree in mechanical and electronic engineering from the Department of Mechanical and Electrical Engineering, Beijing Institute of Technology, in 1998. From November 2006 to November 2007, he was engaged as a state-sponsored Visiting Scholar in digital signal processing research with the Illinois Institute of Technology. From January 2016 to April 2016, he was engaged as a Senior Visiting Scholar in modern measure and detecting technology with The University of Manchester. He is currently a Professor and a Doctoral Supervisor with the North University of China. He is mainly engaged in dynamic testing theory, technology and application, detecting, and digital signal processing technology.

ZHENYU LIN was born in Lvliang, Shanxi, China, in 1995. He received the bachelor's degree in electronic and communication engineering from the North University of China. He is currently pursuing the master's degree in electronic and communication engineering with North China University.

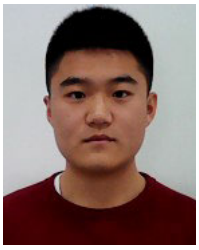

HAOZE CHEN was born in Qinhuangdao, Hebei, China, in 1995. He received the bachelor's degree from the North China Institute of Aerospace Engineering, in 2017. He is currently pursuing the Ph.D. degree in instrument science and technology with the School of Instrument and Electronics. His research interests include non-destructive testing, signal processing, and machine learning.

WULIANG YIN (Senior Member, IEEE) received the B.S. and M.S. degrees in electronic measurement and instrumentation from Tianjin University, Tianjin, China, in 1992 and 1995, respectively, and the Ph.D. degree in automotive electronics from Tsinghua University, Beijing, China, in 1999. He is currently a Lecturer with The University of Manchester, U.K. He has authored or coauthored over 100 publications. His current research interests include advanced sensors and instrumentation, automotive electronics, and electromagnetics. He was a recipient of the Science and Technology Award from the Chinese Ministry of Education, in 2000.